Research Square

Preprints are preliminary reports that have not undergone peer review.
They should not be considered conclusive, used to inform clinical practice,
or referenced by the media as validated information.

Influence of Hexagonal Boron Nitride on the Rheological Behaviour of Concentrated Silica Shear-Thickening Fluids

Sajid Khan
Southeast University
Zhao-Dong Xu
zhdxu@163.com
Southeast University
Yang Yang
Southeast University
Xing-Huai Huang
Southeast University
Chao Xu
Southeast University

Research Article

Keywords: Shear Thickening Fluid (STF), Nanocomposites, SiO_2 (Silica), h-BN (Hexagonal Boron Nitride), Rheological Properties

Posted Date: February 27th, 2026

DOI: https://doi.org/10.21203/rs.3.rs-8264684/v1

License: This work is licensed under a Creative Commons Attribution 4.0 International License. Read Full License

Additional Declarations: No competing interests reported.

Abstract

This study systematically explores the shear-thickening (ST) behavior of silica-based suspensions enhanced with hexagonal-boron-nitride (h-BN) nanoparticles. A series of h-BN/SiO_2 shear-thickening fluids (STFs) with varying concentrations was prepared using mechanical stirring and ultrasonication techniques. The structural and interfacial characteristics of the nanoparticles within the STFs were examined through X-ray diffraction (XRD), transmission electron microscopy (TEM), scanning electron microscopy (SEM), and energy-dispersive spectroscopy (EDS). Steady-shear rheological analyses demonstrated pronounced shear-thickening effects and distinct flow responses across different h-BN loadings. At an optimal concentration of 0.1% h-BN, the critical shear rate decreased by 43.18% (from 17.6 s^{-1} to 10 s^{-1}), while the maximum viscosity increased by 99.2% (from 131.8 Pas to 262.5 Pas). Dynamic oscillatory measurements confirmed that the 0.1% h-BN/SiO_2-STF exhibited superior energy dissipation and storage capabilities, showing predominantly elastic behaviour under low stress, while providing effective energy absorption when subjected to high stress. The formulations also demonstrated excellent reversibility, stability, and minimal temperature dependence, underscoring their potential as intelligent damping materials for impact and vibration control applications. Overall, this work presents a new approach for designing high-performance shear-thickening fluids (STFs) with enhanced rheological and thermal stability characteristics.

1. Introduction

Shear-thickening fluids (STFs) are a class of non-Newtonian materials distinguished by their unique rheological behaviour, in which viscosity increases sharply under high shear stress or sudden impact. These systems are typically composed of dispersed solid particles suspended in a liquid medium, forming a nanocomposite structure. Under normal conditions, STFs exhibit relatively low viscosity; however, when subjected to elevated external forces or high shear rates, particle interactions lead to the formation of hydro-clusters. This results in a marked increase in viscosity, modulus, and other rheological parameters, effectively transforming the STF into a solid-like state [1, 2]. A key feature of STFs is their reversibility, as they readily return to their original liquid state once the applied stress is removed [3], [4], [5], [6]. Additional mechanisms, such as the order-disorder transition of the Hoffman theory, further explain this liquid-solid transition [7]. According to this model, STFs retain an organized, layered structure of particles when subjected to low shear rates. At higher shear rates, however, this lamellar structure collapses into a disordered configuration, leading to an abrupt viscosity increase; a hallmark of shear-thickening (ST) behavior. The jamming theory[8] further explains dilatant shear thickening (DST) in suspensions, where dispersed particles aggregate to form temporary clusters or obstructions that hinder flow. This phenomenon leads to a substantial increase in shear stress and apparent viscosity. Together with other mechanisms, these processes provide a comprehensive understanding of shear-thickening behavior in suspensions. Because of these unique properties, STFs have been modified for various engineering uses, including aerospace. [9], sports apparatus [9, 10], medical and surgical device [11, 12], vibration isolation [13, 14, 15], Protection against impacts at low velocities [16, 17, 18], for the industrial purpose of polishing [19, 20], high-velocity impacts resistance [21, 22], and structural vibration damping [23, 24]. Among these, the most prominent research focus has been on soft body armor for high-velocity impact protection [25, 26, 27]. Incorporating STFs into armor fabrics significantly enhances energy absorption and impact resistance [28, 29]. Consequently, STFs have been widely explored as base materials in diverse industrial applications, including smart fabrics, fibre-reinforced composites, vibration control systems, and ceramic polymers.

The rheological behavior of STFs is governed by various factors, including the shape, size, and distribution of dispersed particles [6, 7],[31] the composition of the suspending medium [8, 9], ambient temperature [10, 11, 12][32], and the mass fraction of dispersed particles [13, 14, 15] 33,34]. Egres et al. [35] investigated the influence of particle morphology on shear-thickening behavior and found that rod-shaped particles exhibited the strongest shear-thickening response, followed by plate-like particles, while spherical particles showed the weakest effect. In addition, irregularly shaped particles, such as calcium carbonate, have been reported to significantly enhance shear-thickening performance due to their structural interactions within the suspension. Similarly, Marazano et al. [36] demonstrated that increasing the mass fraction of dispersed particles raises the initial viscosity of the suspension while lowering the critical shear rate required to induce shear-thickening behavior.

The performance of STFs is also strongly influenced by temperature sensitivity. Wagner et al.[37] Directed a comprehensive investigational study and reported that higher temperatures led to a reduction in the preliminary, minimum, and top viscosities of the suspensions. Increasing the nanoparticle mass fraction in STF systems can further enhance performance, but this often poses challenges due to particle aggregation, which negatively impacts shear-thickening behavior [38]. To overcome these limitations, researchers have explored various approaches, including surface functionalization and chemical or physical modifications, to improve the dispersion stability and optimize rheological properties [16, 17, 18, 19, 20, 21].

Recent progress in STF research has emphasized the incorporation of advanced fillers to enhance performance. For example, Yang et al. [39] demonstrated that introducing particles of different sizes into TiO_2-based suspensions improved viscosity and yield stress, underscoring the significance of particle size distribution. The outcome of TiO_2 suspensions on the rheological behaviour of shearing thickening fluid has been systematically reported in recent studies[40]. Similarly, Tian et al. [41] found SiO_2 (STFs) with the addition of graphene considerably increased viscosity and flow stress at high strain rates, attributed to enhanced forces of hydrodynamic lubrication between nanoparticles. Hwang et al. [42] also reported that incorporating multi-walled carbon nanotubes (MWCNTs) into SiO_2/PEG suspensions significantly enhanced the shear-thickening response by improving both the dispersibility of silica particles and the mechanical properties of MWCNTs. In another study, Gurgen et al. [43] examined the rheological properties of STFs containing ceramic fillers such as boron carbide, aluminium oxide, and silicon carbide across different temperatures. Their results showed systematic variations in suspension properties depending on both type and concentration of ceramic particles.

Functionalized STFs have been developed to meet specific application requirements. For example, Wang et al. [44] incorporated TW-ZnO/SiO_2 whiskers into STF systems to improve the sound insulation properties of STF-impregnated fabrics, achieving superior performance compared to conventional SiO_2-based STFs. Shah et al. [38] reported that graphene nanostructures (GNs) reduced STF viscosity, whereas carbon nanotubes (CNTs) enhanced the shear-thickening

performance. Similarly, Chen et al. [45] showed that CNTs addition not only improved the ST effect but also increased the electrical conductivity of SiO_2-based suspensions. Qiin et al. [46] examined suspensions of Hydrophilic silica in ionic form liquids, demonstrating that the rheological and viscoelastic properties were strongly influenced by the ionic liquid configuration.

Hexagonal boron nitride (h-BN), a two-dimensional layered nanomaterial with a graphene-like hexagonal lattice, has recently attracted attention as a potential STF additive. Its unique combination of high thermal conductivity, electrical insulation, chemical stability, low density, and excellent mechanical strength makes it a promising candidate for enhancing shear-thickening behavior and thermal stability by modulating interparticle interactions and microstructural evolution under shear [47]. Despite these advantages, the application of h-BN in STF systems remains relatively unexplored and represents an important direction for future research [42, 43, 44, 45, 46].

This study investigates the influence of hexagonal boron nitride (h-BN) nanoparticles on the shear-thickening behaviour of silica-based STFs. The h-BN/SiO_2 suspensions were prepared through mechanical stirring and ultrasonication, followed by comprehensive structural and rheological characterization. Steady-shear and oscillatory-shear tests were conducted to evaluate the effects of h-BN mass fraction and ambient temperature on STF performance. For the first time, h-bn nanoparticles were incorporated as a functional nanofiller in silica-based STFs to systematically explore their role in modulating hydroclaster formation, enhancing interparticle interactions, and improving thermal and rheological stability. The incorporation of h-BN is expected to enhance the rheological response and multifunctional properties of silica-based STFs, offering valuable insights for the design of high-performance shear-thickening systems.

2. Experimental Works

2.1 Materials

Silicon dioxide (SiO_2) nanoparticles were purchased from Biochemical Technology Aladdin Co., Ltd. The SiO_2 elements had a middling diameter of 15 nanometres, a pH range of 3.88–4.77, and a relative density of 2.339–2.665. Polyethylene glycol (PEG200) was obtained from Usolf Chemical Technology Co., Ltd. (Shandong, China). At room temperature, PEG200 is a stable, transparent liquid with a hydroxyl value of 510–623 mgKOH/g. hexagonal boron nitride (h-BN) with an average particle size of 100 nm was supplied by Zhen Weld New Materials, Co., Ltd.

2.2 Shear-Thickening Fluids (STFs) preparation

The preparation of shear-thickening fluids (STFs) was carried out in numerous stages to ensure stable rheological performance and uniform particle dispersion. Prior to use, the dispersed-phase particles (nano-SiO_2 and h-BN) were dried in an automated oven at 80°C for 12 h to remove residual moisture. For STF preparation, predetermined amounts of polyethylene glycol (PEG200) and hexagonal boron nitride (h-BN) nanoparticles (0.1% to 0.3 wt%) were placed in a beaker and mixed using a mechanical stirrer. Fumed silica (SiO_2) was then added gradually to the carrier fluid to obtain the desired SiO_2-to-h-BN ratios for each formulation. After each incremental addition of SiO_2, the suspension was stirred for 25 min, while the final stage of mixing was extended to 90 min.

Subsequently, the required amount of h-BN was incorporated, and the suspension was stirred until uniform dispersion was achieved. To maintain consistency during mixing, the beaker was placed in a water bath at a controlled temperature. The mixture was subjected to ultrasonication (40 kHz, 120 W) for 30 min to further enhance particle dispersion within the PEG200 medium. The resulting suspension was transferred to a vacuum chamber and degassed at 110°C for 40 min to eliminate entrapped air bubbles, thereby ensuring a homogeneous composition. The prepared h-BN/SiO_2-based STFs were stored for subsequent rheological characterization. The SiO_2-to-h-BN ratios of the four STF formulations used in this study are summarized in Table 1. Each STF sample was prepared with a constant SiO_2 concentration of 15%, while the h-BN content was varied from 0% to 0.3% to investigate its effect on rheological performance.

Table 1
Composition ratios of the SiO_2 and h-BN nanoparticles in the shear-thickening fluid (STF) systems.

Sample ID	Dispersed Phase Composition	Mass Ratio (% w/w)
Reference	15% + 0% h-BN	15:0
Sample 1	15% + 0.1% h-BN	15:0.1
Sample 2	15% + 0.2% h-BN	15:0.2
Sample 3	15% + 0.3% h-BN	15:0.3
Note: PEG200 was used as the dispersing medium in all STF formulations		

2.3 Rheological Testing

The rheological properties of the prepared h-BN/SiO_2-based STFs with varying SiO_2-to-h-BN ratios were investigated under steady-shear and dynamic conditions using a rheometer (AR2000, TA Instruments, USA). All tests were conducted at a controlled ambient temperature of 18°C. A cone-plate geometry with a 25 mm diameter and 2° cone angle was employed, and the measurement gap was maintained at 52 μm. Before testing, STF samples were evenly distributed on the bottom plate of the rheometer. The upper conc was then lowered to achieve the required 52 μm gap. Temperature regulation during the

experiments was maintained using the integrated control system of the rheometer. To evaluate thermal sensitivity, rheological measurements were conducted at 15, 20, 30, 40, and 50°C.

Steady-shear tests were conducted over a shear rate range of 0.1-1000s^{-1}, enabling analysis of shear-thickening behavior, including the critical shear rate and viscosity variation under varying stress levels. Dynamic rheological testing involved applying oscillatory shear stresses from 0.1 to 1000 Pa. These tests provided insights into the viscoelastic properties of the STFs, including energy storage and dissipation behavior under both low- and high-stress conditions. By combining steady-shear and oscillatory measurements, a comprehensive evaluation of the shear-thickening response, viscoelasticity, and temperature dependence of the h-BN/SiO_2-based STFs was achieved. Such findings are essential for optimizing STF formulations for advanced engineering applications.

3. Results and Discussion

3.1 Microscopic Characterization of STF Materials

The SiO_2, h-BN, and h-BN/SiO_2 samples were prepared by dispersing the appropriate amounts in absolute ethanol, followed by ultrasonication to achieve uniform distribution. The suspensions were deposited onto copper foil substrates, dried completely, and then coated with gold for 60 s using a sputter coater to ensure conductivity before scanning electron microscopy (SEM) analysis. SEM observations were conducted using a Nova Nano SEM 450.

Figure 1 presents the SEM micrographs of the samples. As shown in Fig. 1**(a)**, the SiO_2 particles exhibit a uniform, fine-grained morphology at the nanoscale, which promotes homogeneous dispersion in the STF matrix and minimizes performance variations caused by particle size distribution. In Fig. 1**(b)**, h-BN displays a characteristic plate-like morphology with a layered structure. This structural feature is particularly significant for enhancing thermal conductivity and providing mechanical reinforcement, as the layered architecture facilitates efficient heat dissipation and strengthens the composite. Figure 1**(c)** depicts the h-BN/SiO_2 composite, where clear interfacial interactions between SiO_2 nanoparticles and h-BN sheets were observed. The combination of the granular morphology of SiO_2 with the layered structure of h-BN contributes to improved interfacial bonding, reduced agglomeration, and enhanced overall stability. These synergetic effects are expected to contribute to the superior thermal and mechanical performance of the STF system.

Energy-dispersive spectroscopy (EDS) mapping was carried out to examine the elemental distribution and confirm the presence of constituents in the h-BN/SiO_2 composite, as presented in Fig. 2. Figure 2**(a)** demonstrates the uniform dispersion of particles throughout the sample, with no evidence of clustering. The elemental mapping presented in Fig. 2**(b)** indicates the even distribution of Si, O, B, and N, confirming the coexistence of SiO_2 and h-BN within the composite. Quantitative EDS analysis revealed atomic fractions of Si (56.30%), O (29.15%), B (10.66%), and N (3.89%). Notably, no carbon peaks were detected, verifying the purity of the composite and the absence of significant contamination. As illustrated in Fig. 2**(c)**, the calculated atomic ratios further confirm the successful integration of SiO_2 and h-BN, validating the well-structured and homogeneous.

HR-TEM analysis was employed to find the morphology and crystal parameters of the synthesized samples. The HR-TEM images show that in Fig. 3 **(a)**, much of the silica (SiO_2) nanoparticles appeared spherical with good monodispersity. Most particles were well-dispersed and existed independently in the medium, indicating a low viscosity of the suspension. As shown in Fig. 3**(b)**, the BN nanoparticles display a relatively uniform morphology with minimal agglomeration. The particle size of the nanomaterials was measured using Image J software. The average particle sizes of approximately 125 nm, consistent with nanoscale morphology. While the nano h-BN/SiO_2 composite exhibits an irregular morphology with some degree of aggregation, this indicating that the particles are not fully dispersed in the medium. The image shows a combination of SiO_2 and hBN structures, where hBN nanoparticles appear to be attached to or embedded within the silica particles, as shown in Fig. 3**(c)**. The size of the composite particles appears larger compared to the individual SiO_2 and hBN particles, likely due to the aggregation. However, based on the scale bar in the image (1 μm), the particle size can be estimated to be in the range of 100–300 nm, with some larger aggregates possibly exceeding this size. The HR-TEM images of SiO_2, h-BN and nano h-BN/SiO_2 composite at different magnification are presented in **Fig. S2** in the supporting information.

The crystalline phases of the samples were analysed using an X-ray diffractometer (D8-Discover) equipped with a Cu target source. The operating parameters were set to 40 kV voltage, 35 mA current, a step size of 0.044°, a scanning speed of 8°/min, and a scanning angle range of 5°-90°. The corresponding XRD patterns are presented in Fig. 4. The silicon dioxide (SiO_2) sample displayed a wide diffraction top between 20° and 30°, characteristic of its amorphous structure. In contrast, h-BN displayed sharp peaks at 26°, 41°, 55°, and 76°, confirming its well-defined hexagonal crystalline structure. The diffraction pattern of the h-BN/SiO_2 composite largely resembled that of h-BN; however, the peak intensities were reduced, suggesting that the composite retained a predominantly crystalline nature with modified structural characteristics. These outcomes authorize the success of h-BN and SiO_2, underscore the potential of the composite material for advanced functional applications.

3.2 Analysis of STFs under constant shear conditions

Figure 5**(a and b)** and Figs. 6 presents the viscosity profiles of h-BN/SiO_2-based shear-thickening fluids (STFs) obtained from steady-state shear tests conducted over a shear rate range of 0.1–1000 s^{-1} for four different mass ratios. All formulations used PEG200 as the dispersion medium, with h-BN mass portions of 0%, 0.1%, 0.2%, and 0.3%, while maintaining a constant SiO_2 concentration of 15%. Each viscosity curve exhibits three distinct regions: an initial shear-thinning phase characterized by a rapid decrease in viscosity, followed by a shear-thickening region, and finally another shear-thinning stage at higher shear rates. The incorporation of h-BN nanoparticles significantly influenced the rheological response of the STFs. Compared to the SiO_2-only system, the h-BN/SiO_2-STFs exhibited higher apparent viscosity and a more noticeable shear-thickening effect. This enhancement can be attributed to the synergistic interaction between h-BN sheets and SiO2 particles, which promotes the formation of stronger transient particle networks under shear, thereby improving energy dissipation and resistance to deformation.

The addition of h-BN to the system resulted in a significant in overall viscosity, particularly beyond the critical shear rate, as h-BN particles clustered around functional groups, Impeding the free movement of particles. aggregates. However, the viscosity trends varied with different h-BN mass fractions. At 0.1% h-BN, the system exhibited the optimal balance between viscosity and shear-thickening performance, as shown in Table 2. The critical shear rate decreased significantly, from 17.6 s^{-1} to 10 s^{-1}, while the peak viscosity nearly doubled, from 131.8 Pas to 262.5 Pas, marking a 99.2% improvement over the SiO_2-only system (0% h-BN/15% SiO_2). This enhancement is attributed to increased particle interactions and reduced interparticle spacing. However, the viscosity enhancement diminished at higher h-BN concentrations (0.2% and 0.3%), likely due to two factors: (i) particle agglomeration caused by stronger van der Waals forces between h-BN sheets, which disrupt the internal network of the STF, and (ii) excessive lubrication resulting from the smooth surface and high thermal conductivity of h-BN, which reduces interparticle friction. Similar trends have been observed with nano-ZrO_2 [53], where lower concentrations improved lubrication and reduced SiO_2 particle interactions, thereby lowering the critical shear rate, while higher concentrations hindered network formation and raised the critical shear rate. These findings emphasize the need to optimize nanoparticle concentration for effective shear-thickening behavior.

Table 2
Rheological parameters of h-BN/SiO_2-based shear-thickening fluids (STFs).

Samples No	h-BN/SiO_2 Composition	Initial Viscosity (Pa.s at 0.11 s^{-1})	Critical Viscosity (Pa.s at s^{-1})	Peak Viscosity (Pa.s at s^{-1})
Reference	0% h-BN + 15% SiO_2	5.4 (0.11 s^{-1})	3.7 (17.6 s^{-1})	131.8 (53.9 s^{-1})
Sample 1	0.1% h-BN + 15% SiO_2	7.6 (0.11 s^{-1})	5.5 (10.0 s^{-1})	262.5 (31 s^{-1})
Sample 2	0.2% h-BN + 15% SiO_2	7.4 (0.11 s^{-1})	5.5 (10.0 s^{-1})	246.1 (31.1 s^{-1})
Sample 3	0.3% h-BN + 15% SiO_2	6.1 (0.11 s^{-1})	4.2 (13.3 s^{-1})	176.6 (53.9 s^{-1})

To demonstrate the enhancement in the viscosity of the STFs, we define the following ratio:

$$\text{Percentage Increase} = \frac{\text{Max Viscosity(A)} - \text{Max Viscosity(B)}}{\text{Max Viscosity(B)}} \%$$

Viscosity A indicates the peak values of trials sample one, sample two, and sample three, although B denotes the peak viscosity exhibited by the initial sample throughout the shear thickening transition. The results are presented in Fig. 5**(c)**.

Increasing the h-BN concentration beyond 0.1% resulted in a decrease in peak viscosity and an increase in critical shear rates, likely due to excessive particle dispersion and lubrication effects. For example, at 0.3% h-BN, the critical shear rate has risen. to 13.3 s^{-1}, while the highest viscosity reduced to 176.6 Pas. These findings highlight the optimization of h-BN concentration to achieve a balance between shear-thickening behaviour and flowability, with 0.1% h-BN recognized as the best composition.

The reversibility and stability of the STF were also evaluated. Figure 7**(a)** shows the reversible nature of the STFs, showing minimal hysteresis between viscosity curves during cyclic shear tests. This reversibility is attributed to the transient particle clustering behaviour under varying shear forces. Stability tests, as shown in Fig. 7**(b)**, revealed that viscosity remained largely stable under steady shear conditions, confirming the STF's reliability for extended use.

3.3 Analysis of STF's Dynamic Rheology

The dynamic rheological properties of the 0.1% h-BN/SiO_2-STF system was evaluated to investigate its viscoelastic response under varying strain conditions. Figure 5**(c and d)** shows the variation of the loss modulus (G") and storage modulus (G') with strain at 10, 25, 50, and 100 rad/s of angular frequencies. The system exhibited four distinct stages: an initial elastic region, followed by an initial slight thinning phase, then a pronounced thickening stage, and concluding with a final thinning phase. With increasing strain, both G' and G" exhibited an overall upward trend, indicating the effect of uniform particle dispersion and the formation of transient particle clusters within the suspension.

The frequency-dependent variation of the storage modulus (G') and loss modulus (G") is indicated in Fig. 7**(c and d)**. At low angular frequencies, the Brownian motion and intermolecular forces helped maintain the structure of the suspension, resulting in a gradual increase in both moduli. As the frequency increased, hydrodynamic lubrication effects facilitated particle clustering, leading to a nonlinear rise in modulus values. These observations highlights the STF's strong energy dissipation capability under dynamic loading, underscoring its potential for vibration damping and impact absorption applications.

The dynamic rheological performance of the 0.1% h-BN/SiO_2-based shear-thickening fluid (STF) was evaluated under oscillatory loading conditions. Figure 7 illustrates the evolution of the storage modulus (G') and loss modulus (G") at different angular frequencies (10, 25, 50, and 100 rad/s) as the strain amplitude increased. The system exhibited four distinct rheological stages: (i) an initial elastic regime at low strains; (ii) a mild shear-thinning response; (iii) a strong shear-thickening transition marked by sharp increases in both G' and G"; and (iv) a secondary shear-thinning stage associated with structural disintegration. These observations align with the findings of Wei et al., [54] for CeO_2/SiO_2-STFs, who reported similar transitions with increasing strain. The enhanced energy dissipation and greater modulus sensitivity during the thickening phase can be attributed to the uniform particle dispersion and stable network formation within the suspension.

As shown in Fig. 8**(a and b)**, frequency-dependent variation of G' and G" further clarifies the system's dynamic response. At lower angular frequency, Brownian motion and weak intermolecular interactions dominate, enabling effective structural reorganization. At higher frequencies, hydrodynamic lubrication forces promote particle clustering, increasing internal resistance and causing nonlinear growth in both moduli. This hydro-lubrication-induced clustering has also

been observed in CeO_2/SiO_2-STFs, suggesting a universal mechanism among nanoparticles-reinforced STFs. Notably, G' remained consistently higher than G" across all frequencies, particularly at elevated ones, indicating the fluid's strong viscous dissipation tendency. This dominance of the loss modulus underscores the material's excellent energy absorption potential, making it suitable for impact mitigation and damping applications. Furthermore, the incorporation of h-BN was found to significantly influence particle clustering and internal friction characteristics. The 0.1% h-BN loading produced a comparable rheological enhancement at a much lower concentration than CeO_2/SiO_2 systems, which typically require ~ 12% ceria for peak performance. This efficiency arises from h-BN's high aspect ratio and smooth surface, which facilitate both lubrication and microstructural development. However, higher h-BN concentrations led to reduced performance because of particle agglomeration and excessive lubrication, and consistent with trends observed in zirconia-modified systems [53]. Overall, these findings demonstrate the dynamic adaptability and tunable rheological response of h-BN-reinforced STFs, reinforcing their potential as next-generation materials for structural damping, vibration control, and advanced protective systems.

3.4 STF Temperature Sensitivity

Figures 9 **(a, b, c and d)** illustrate the relationship between shear rate and viscosity at different temperature for the 0.1% h-BN/SiO_2-STF and 0% h-BN/SiO_2-STF systems, respectively. Both systems exhibited a reduction in initial and peak viscosities with increasing temperature, accompanied by a shift toward higher critical shear rates. Nonetheless, the 0.1% h-BN-modified STF consistently demonstrated superior rheological performance compared to the unmodified system across all tested temperatures. At 15°C, the 0.1% h-BN/SiO_2-STF achieved a peak viscosity of 263 Pas and a critical shear rate of $10s^{-1}$, corresponding to a 99.05% enhancement in viscosity along with a 42.49% reduction in critical shear rate compared to the 0% h-BN system. Even at 50°C, the 0.1% h-BN enhanced STF maintained a 43.32% higher viscosity and a 42.24% lower critical shear rate, confirming its thermal resilience and consistent shear-thickening response [47]. The improved temperature stability of the h-BN-based STF can be attributed to the strong particle-polymer interactions within the PEG-h-BN matrix, which remain effective over the temperature range of 15–50°C. The presence of h-BN likely acts as a thermal stabilizer by restricting molecular mobility within the matrix, thereby preserving the structural integrity necessary for shear-thickening behavior. These observations align well with prior studies [53], [54], further validating the effectiveness of h-BN as a functional additive for enhancing the thermal and rheological stability of STFs in high-temperature or dynamic environments.

3.5 Evaluation of mathematical model fitting for (STFs)

3.5.1 Model for STFs

In the literature, many researchers have developed phenomenological and empirical models to describe the rheological behaviour of steady-state shear-thickening fluids—notably, the model introduced by Galindo-Rosales et al.[55] It accurately captures the full rheological behaviour of shear thickening. This mathematical model effectively characterizes and observes the three standard flow systems: (i) at minimum shear rates, initial shear-thinning behaviour, (ii) shear-thickening observed within a specific shear rate range, and lastly (3) there is again a region of shear thinning occur when the shear rate becomes high. The corresponding revised design is expressed as follows **Eq. 1.**

$$\eta(\dot{\gamma}) = \begin{cases} \eta_1(\dot{\gamma}) = \eta_c + \dfrac{\eta_0 - \eta_c}{1 + \left|\left[\mathbf{K}_1\left(\dot{\gamma}^2/(\dot{\gamma} - \dot{\gamma}_c)\right)\right]\right|^{n_1}} \\ \eta_2(\dot{\gamma}) = \eta_{max} + \dfrac{\eta_c - \eta_{max}}{1 + \left|\left[\mathbf{K}_2\left((\dot{\gamma} - \dot{\gamma}_c)/(\dot{\gamma} - \dot{\gamma}_{max})\right)\dot{\gamma}\right]\right|^{n_2}} \\ \eta_3(\dot{\gamma}) = \dfrac{\eta_{max}}{1 + \left|\left[\mathbf{K}_3\left((\dot{\gamma} - \dot{\gamma}_{max})\right)\right]\right|^{n_3}} \end{cases} \quad f$$

1

The parameters enclosed within the absolute-value notation ensure non-negative inputs, enabling the stable evaluation of terms involving fractional exponents. In this model, ηmax refers to the peak viscosity, η_0 refers to the viscosity at which the shear rate is almost zero, and ηc refers to the viscosity at which the shear rate becomes critical. Likewise, γ̇c and γ̇max symbolise the critical shear rate marking the beginning of thickening and the shear rate at which maximum viscosity occurs, respectively. The coefficient K_i, K_{ii}, and K_{iii} serves as rate constants leading each flow regime, whereas the exponents n_i, n_{ii}, and n_{iii} are the parameters that don't have dimensions and define the viscosity slope profile across the different rheological regions.

1.1.2 Impact of h-BN Concentration on Modelling Accuracy

All the parameters used in this model, like $\dot{\gamma}c$, $\dot{\gamma}$max, ηo, ηc, ηmax, for PEG200/h-BN/(STFs) containing 0%, 0.1%, 0.2%, and 0.3% h-BN have been previously summarized in. Table 2. These rheological indicators provide essential insight into how the fluid response evolves under varying shear conditions.

To characterize this behaviour, the relationship between shear rate and viscosity was fitted using the constitutive law of Galindo-Rosales. **Eq. 1** effectively imprisons both the region of thickening and thinning. Through least square regression, all the model parameters are determined among the predicted and experimental values, and the deviation is reduced to confirm an accurate representation along the entire range of shear rate.

All the shape parameters of the model (Ki, Kii, Kiii, ni, nii, and niii) obtained by nonlinear regression are indicated in the form of Table 3. Reflecting the magnitude and progression of shear thickening behaviour for each composition. Figure 10 compares the experimental viscosity curves with model predictions for h-BN concentrations of 0%, 0.1%, 0.2%, and 0.3%.

Table 3
Viscosity function parameter

Parameters	0%h-Bn	0.1%h-Bn	0.2%h-Bn	0.3%h-Bn
N_i	1.206464664	1.2643561043	1.206464664	1.175720168
N_{ii}	0.570940998	1.102194377	0.570940998	0.561885377
N_{ii}	2.485630942	3.000345485	2.485630942	2.017907581
K_i	0.022465278	0.121771612	0.022465278	0.047893439
K_{ii}	0.376571819	0.410480064	0.376571819	0.2604465
K_{iii}	0.007763063	0.007978288	0.007763063	0.009173796

1.2 Comparison of Experimental Data with Model Predictions

Because of its quick convergence and resilience in solving the nonlinear least-squares problem, model parameters were obtained through curve fitting using the Levenberg-Marquardt method. This hybrid optimization method, which integrates features of both the steepest descent and Gauss-Newton approaches, iteratively reduces the (χ^2) values till the difference between subsequent iterations is less than 10^{-9}. The Early constraint guesstimates were selected based on the investigational shear rate- viscosity trends to ensure stable and accurate convergence for each STF formulation.

Using the corresponding parts of the consistent model, the fitting process was carried out in regions afterwards. The configurations that were optimized (Ki, K2, K3, ni, n2, and n3) for h-Bn concentrations of 0%, 0.1%, 0.2%, and 0.3% are summarized in Table 3. This phenomenological model exhibits strong correlation with the investigational data, with R2 values ranging from 0.9891 to 0.9981 and the values of RMSE between 0.05 and 0.18, confirming its reliability and accuracy.

The incorporation of h-BN remarkably exaggerated the behaviour of fitting by improving the intensity of shear-thickening and promoting high growth of viscosity near the point of critical shear rates. Among all samples, the formulation containing 0.1% h-BN produced the most accurate fitting (R^2 = 0.989, RMSE = 0.04976), at this concentration, suggesting optimum dispersibility of nanoparticle and hydroclaster formation. Inclusive, R2 values are typically high (> 0.99) all trails verify the model's ability to capture the h-BN-STFs nonlinear rheological behaviour.

4. Conclusions

This study observed h-BN/SiO_2-based shear-thickening fluids (STFs) with varying mass ratios, focusing on their rheological behavior, temperature sensitivity, reversibility, and microstructural characteristics. All formulations exhibited distinct shear-thickening (ST) behavior, with the incorporation of hexagonal boron nitride (h-BN) nanoparticles significantly enhancing the apparent viscosity and overall rheological performance of the SiO_2-based STFs. Among the tested systems, the 0.1% h-BN/SiO_2-STF demonstrated the most favorable balance between peak viscosity and critical shear rate, confirming it as the optimal formulation. Although elevated temperature influenced viscosity and shear-thickening intensity, the 0.1% h-BN/SiO_2-STF system maintained consistent performance and excellent reversibility under cyclic loading, reflecting its thermal stability and durability. These conclusions emphasize the reputation of optimizing h-BN concentration to achieve superior rheological and thermal properties. The 0.1% h-BN/SiO_2-STF composition shows strong potential for advanced applications in impact mitigation, vibration control, and protective systems. Future work should further explore the effects of nanoparticle size, morphology, and dispersion strategies on STF performance across diverse operating conditions.

Authors Statement

All authors made equal contributions to this work.

Declarations

Competing Interests

The authors declare no competing financial or non-financial. interests related to this work.

Figure 1

SEM micrographs showing the surface morphology of **(a)** nano-SiO_2 particles, (b) nano-h-BN particles, and (c) the nano-h-BN/SiO_2 composite.

Figure 3

HR-TEM images of (a) SiO2 nanoparticles, (b) h-BN nanoparticles, and (c) nano h-BN/SiO_2 composite

Figure 4

The XRD diffraction profile of SiO_2, h-BN, and h-BN/SiO_2 composite powders.

Figure 5

For the h-BN-SiO_2/STF system prepared with varying h-BN-to-SiO_2 ratios, viscosity vs shear rate is illustrated using (a) Log graph, (b) half Log graph, and (c) Comparative analysis for numerous h-BN shear-thickening fluids.

Figure 6

For the h-BN-SiO_2/STF system with different h-BN ratios, Stress against shear rate. (a) Logarithmic graph. (b) Semi-Logarithmic graph.

Figure 7

Rheological characteristics of the 0.1%h-BN/SiO_2-STF shear thickening fluid sample (a) Reversibility, (b) Stability, (c) Strain versus storage and loss modulus for 0.1%h-BN/SiO_2-STF Coordinate logarithm, and (d) Semi-coordinate Logarithm.

Figure 8

Storage and loss modulus for 0.1% h-BN/SiO_2-STF as a frequency function, (a) Logarithmic, and (b) Semi-logarithmic.

Figure 9

Shear rate against viscosity for 0.1%h-BN/SiO_2-STF. at different temperatures, (a) Logarithmic, (b) Semi-logarithmic, (c) Shear rate against viscosity for 0% h-BN/SiO_2-STF. to varying temperatures of coordinate. Logarithm, and (d) Semi-logarithmic.

Figure 10

Comparison between experimental results and the model for various h-Bn percentages, including 0%, 0.1%, 0.2%, and 0.3%.

Table 1

Composition ratios of the SiO_2 and h-BN nanoparticles in the shear-thickening fluid (STF) systems.

Table 2

Rheological parameters of h-BN/SiO_2-based shear-thickening fluids (STFs).

Author Contribution

All authors made equal contributions to this work.

Acknowledgments

This. research was supported by funding from the Shenzhen Science.and Technology Program (Grant No. KCXFZ20211020165543004) and the Natural Science Foundation. of Jiangsu. Higher. Education Institutions of China (Grant No. 23KJB130003). The authors express their gratitude for this support, which was instrumental in enabling the successful. completion. of this study.

References

1. Tian T, Nakano M (Mar. 2017) Design and testing of a rotational brake with shear thickening fluids. Smart Mater Struct 26(3):035038. 10.1088/1361-665X/aa5a2c
2. Brown E, Jaeger HM (2014) Shear thickening in concentrated suspensions: phenomenology, mechanisms and relations to jamming. Rep Prog Phys 77(4). 10.1088/0034-4885/77/4/046602

3. Waitukaitis SR, Jaeger HM (2012) Impact-activated solidification of dense suspensions via dynamic jamming fronts, *Nature 2012 487:7406*, vol. 487, no. 7406, pp. 205–209, Jul. 10.1038/nature11187
4. Lu Z, He X, Zhou Y (Aug. 2018) Performance-based seismic analysis on a super high-rise building with improved viscously damped outrigger system. Struct Control Health Monit 25(8):e2190. 10.1002/stc.2190
5. Lu Z, Wang Z, Zhou Y, Lu X (Jun. 2018) Nonlinear dissipative devices in structural vibration control: A review. J Sound Vib 423:18–49. 10.1016/j.jsv.2018.02.052
6. Huseynov EM, Naghiyev TG, Abbasov NR (May 2022) The paramagnetic approach of the color-changing of nano h-BN particle under the neutron irradiation. Phys E Low Dimens Syst Nanostruct 139:115124. 10.1016/j.physe.2021.115124
7. Hoffman RL (1972) Discontinuous and Dilatant Viscosity Behavior in Concentrated Suspensions. I. Observation of a Flow Instability, *Transactions of the Society of Rheology*, vol. 16, no. 1, pp. 155–173, Mar. 10.1122/1.549250
8. Olsson P, Teitel S (Oct. 2007) Critical Scaling of Shear Viscosity at the Jamming Transition. Phys Rev Lett 99:178001. 10.1103/PhysRevLett.99.178001
9. Zarei M, Aalaie J (Sep. 2020) Application of shear thickening fluids in material development. J Mater Res Technol 9(5):10411–10433. 10.1016/j.jmrt.2020.07.049
10. Cossa KN (Oct. 2019) Basic concepts on rheology and application of shear-thickening fluids in protective gear. SN Appl Sci 1(10):1–6. 10.1007/S42452-019-1315-5/METRICS
11. Laifa S, Tria DE, Derradji M, Khalfallah S (2023) The synergistic effect of temperature and loading rate on the mechanical behavior of shear thickening fluid reinforced with graphene nano-platelets using split Hopkinson pressure bar, *Thin-Walled Structures*, vol. 192, p. 111133, Nov. 10.1016/j.tws.2023.111133
12. Ding J, Tracey P, Li W, Peng G, Whitten P, Wallace G (2013) Review on shear thickening fluids and applications, Jan. Accessed: May 12, 2025. [Online]. Available: /articles/journal_contribution/Review_on_shear_thickening_fluids_and_applications/27710034/1
13. Surgical (2007) and medical garments and materials incorporating shear thickening fluids. Sep
14. Gürgen S, Kuşhan MC, Li W (2017) Shear thickening fluids in protective applications: A review, *Prog Polym Sci*, vol. 75, pp. 48–72, Dec. 10.1016/j.progpolymsci.2017.07.003
15. Liu H, Fu K, Cui X, Zhu H, Yang B (May 2023) Shear Thickening Fluid and Its Application in Impact Protection: A Review. Polym (Basel) 15(10):2238. 10.3390/polym15102238
16. Sheikhi MR, Sofuoğlu MA, Chen Z (2023) Shear Thickening Fluid Integrated Sandwich Structures for Vibration Isolation. in Shear Thickening Fluid. Springer International Publishing, Cham, pp 27–40. doi: 10.1007/978-3-031-35521-9_3.
17. Sun L, Wei M, Zhu J (Apr. 2021) Low velocity impact performance of fiber-reinforced polymer impregnated with shear thickening fluid. Polym Test 96:107095. 10.1016/j.polymertesting.2021.107095
18. Lim J, Kim S-W (Oct. 2023) Low-velocity impact responses of composite structures incorporating shear thickening fluid tubes under various temperatures. Compos Struct 322:117349. 10.1016/j.compstruct.2023.117349
19. Decker MJ, Halbach CJ, Nam CH, Wagner NJ, Wetzel ED (2007) Stab resistance of shear thickening fluid (STF)-treated fabrics, *Compos Sci Technol*, vol. 67, no. 3–4, pp. 565–578, Mar. 10.1016/j.compscitech.2006.08.007
20. Lyu BH, He QK, Chen SH, Shao Q, Chen Y, Geng ZY (2019) Experimental study on shear thickening polishing of cemented carbide insert with complex shape, *The International Journal of Advanced Manufacturing Technology*, vol. 103, no. 1–4, pp. 585–595, Jul. 10.1007/s00170-019-03600-w
21. Shao Q, Lyu B, Yuan J, Wang X, Ke M, Zhao P (2021) Shear thickening polishing of the concave surface of high-temperature nickel-based alloy turbine blade, *Journal of Materials Research and Technology*, vol. 11, pp. 72–84, Mar. 10.1016/j.jmrt.2020.12.112
22. Wang X, Zhang J, Bao L, Yang W, Zhou F, Liu W (Nov. 2020) Enhancement of the ballistic performance of aramid fabric with polyurethane and shear thickening fluid. Mater Des 196:109015. 10.1016/j.matdes.2020.109015
23. Lee YS, Wetzel ED, Wagner NJ (2003) The ballistic impact characteristics of Kevlar® woven fabrics impregnated with a colloidal shear thickening fluid. J Mater Sci 38(13):2825–2833. 10.1023/A:1024424200221
24. Rauf Sheikhi M et al (Nov. 2023) Design of smart sandwich structures enhanced by multi-functional shear thickening fluids (M – STFs): Anti-vibration and electrical conductivity. Compos Struct 324:117520. 10.1016/j.compstruct.2023.117520
25. G. Haydarlar, M. A. Sofuoğlu, S. Gürgen, M. C. Kushan, and M. Tekkalmaz, An Electromechanical*In Situ* Viscosity Measurement Technique for Shear Thickening Fluids,*Advanced Engineering Forum*, vol. 43, pp. 33–43, Nov. 2021, doi: 10.4028/www.scientific.net/AEF.43.33
26. Bajya M, Majumdar A, Butola BS, Verma SK, Bhattacharjee D (Feb. 2020) Design strategy for optimising weight and ballistic performance of soft body armour reinforced with shear thickening fluid. Compos B Eng 183:107721. 10.1016/j.compositesb.2019.107721
27. Lu Z, Yuan Z, Chen X, Qiu J (Nov. 2019) Evaluation of ballistic performance of STF impregnated fabrics under high velocity impact. Compos Struct 227:111208. 10.1016/j.compstruct.2019.111208
28. Ribeiro MP, da Silveira PHPM, de Oliveira F, Braga, Monteiro SN (Oct. 2022) Fabric Impregnation with Shear Thickening Fluid for Ballistic Armor Polymer Composites: An Updated Overview. Polym (Basel) 14(20):4357. 10.3390/polym14204357
29. Wu S, Sikdar P, Bhat GS (2023) Recent progress in developing ballistic and anti-impact materials: Nanotechnology and main approaches, *Defence Technology*, vol. 21, pp. 33–61, Mar. 10.1016/j.dt.2022.06.007
30. Kim Y, Sathish Kumar SK, Park Y, Kwon H, Kim C-G (2020) High-velocity impact onto a high-frictional fabric treated with adhesive spray coating and shear thickening fluid impregnation, *Compos B Eng*, vol. 185, p. 107742, Mar. 10.1016/j.compositesb.2020.107742

31. Huseynov EM, Jazbec A (Oct. 2024) Application of neutron transmutation technology to control the physical properties of nanoparticles at the atomic scale. Carbon N Y 229:119568. 10.1016/j.carbon.2024.119568
32. Huseynov EM, Naghiyev TG (2022) Various thermal parameters investigation of 3C-SiC nanoparticles at the different heating rates, *Applied Physics A*, vol. 128, no. 2, p. 115, Feb. 10.1007/s00339-022-05265-x
33. Huseynov EM, Valizade AH (May 2025) EPR investigation of structural changes in nanocrystalline 3C-SiC under gamma irradiation. Ceram Int 51(13):17379–17386. 10.1016/j.ceramint.2025.01.510
34. Huseynov EM, Atakishiyeva JG (Aug. 2024) Characterizing neutron irradiation-induced effects in the nanocrystalline B4C particles using EPR spectroscopy. Solid State Sci 154:107604. 10.1016/j.solidstatesciences.2024.107604
35. Egres RG, Wagner NJ (May 2005) The rheology and microstructure of acicular precipitated calcium carbonate colloidal suspensions through the shear thickening transition. J Rheol (N Y N Y) 49(3):719–746. 10.1122/1.1895800
36. Maranzano BJ, Wagner NJ (2001) The effects of interparticle interactions and particle size on reversible shear thickening: Hard-sphere colloidal dispersions, *J Rheol (N Y N Y)*, vol. 45, no. 5, pp. 1205–1222, Sep. 10.1122/1.1392295
37. Wagner NJ, Brady JF (Oct. 2009) Shear thickening in colloidal dispersions. Phys Today 62(10):27–32. 10.1063/1.3248476
38. Sha X, Yu K, Cao H, Qian K (Jul. 2013) Shear thickening behavior of nanoparticle suspensions with carbon nanofillers. J Nanopart Res 15:1816. 10.1007/s11051-013-1816-x
39. Yang HG, Li CZ, Gu HC, Fang TN (Apr. 2001) Rheological Behavior of Titanium Dioxide Suspensions. J Colloid Interface Sci 236(1):96–103. 10.1006/JCIS.2000.7373
40. Khan S, Xu Z-D, Hussain I, Xu Y, Huang X-H, SUN B (Nov. 2025) Rheological Performance of Titanium Oxide Nanoparticles on Silica-Based Shear-Thickening Fluids. Surf Interfaces 108122. 10.1016/J.SURFIN.2025.108122
41. Tan Z, Ma H, Zhou H, Han X, Cho C (2019) The influence of graphene on the dynamic mechanical behaviour of shear thickening fluids, *Advanced Powder Technology*, vol. 30, no. 10, pp. 2416–2421, Oct. 10.1016/j.apt.2019.07.025
42. Y. W. K. JYL, Hwang YHKHN, PREPARATION OF SILICA-COATED MWNTS AND THEIR ADDITION TO SHEAR THICKENING FLUID OF SILICA/PEG SUSPENSION (2009), *18TH INTERNATIONAL CONFERENCE ON COMPOSITE MATERIALS*
43. Gürgen S, Li W, Kuşhan MC (Aug. 2016) The rheology of shear thickening fluids with various ceramic particle additives. Mater Des 104:312–319. 10.1016/j.matdes.2016.05.055
44. Wang Y et al (2015) Effect of TW-ZnO/SiO2-compounded shear thickening fluid on the sound insulation property of glass fiber fabric. Text Res J 85(9):980–986. 10.1177/0040517514561925
45. Chen Q, Liu M, Xuan S, Jiang W, Cao S, Gong X (May 2017) Shear dependent electrical property of conductive shear thickening fluid. Mater Des 121:92–100. 10.1016/J.MATDES.2017.02.056
46. Qin J, Zhang G, Ma Z, Li J, Zhou L, Shi X (2016) Effects of ionic structures on shear thickening fluids composed of ionic liquids and silica nanoparticles. RSC Adv 6(85):81913–81923. 10.1039/C6RA12460G
47. Kong X et al (Jan. 2022) Two-Dimensional Hexagonal Boron Nitride Nanosheets as Lateral Heat Spreader With High Thermal Conductivity. Front Mater 8. 10.3389/fmats.2021.817061
48. Jiang H et al (Jan. 2024) Recent research advances in hexagonal boron nitride/polymer nanocomposites with isotropic thermal conductivity. Adv Nanocomposites 1(1):144–156. 10.1016/J.ADNA.2024.03.004
49. Kostoglou N et al (Dec. 2020) Boron Nitride Nanotubes Versus Carbon Nanotubes: A Thermal Stability and Oxidation Behavior Study. Nanomaterials 10(12):2435. 10.3390/nano10122435
50. Zhang Y, Wang Y, Qin C, Cao J (2024) Synthesis and modification of boron nitride nanomaterials for gas sensors: from theory to application. Phys Chem Chem Phys 26(45):28307–28331. 10.1039/D4CP02137A
51. Gadore V, Mishra SR, Singh AK, Md, Ahmaruzzaman (2024) Advances in boron nitride-based nanomaterials for environmental remediation and water splitting: a review. RSC Adv 14(5):3447–3472. 10.1039/D3RA08323C
52. Wen W et al (Mar. 2018) Recent advances in emerging 2D nanomaterials for biosensing and bioimaging applications. Mater Today 21(2):164–177. 10.1016/j.mattod.2017.09.001
53. Sun L, Zhu J, Wei M, Zhang C, Song Y, Qi P (May 2018) Effect of zirconia nanoparticles on the rheological properties of silica-based shear thickening fluid. Mater Res Express 5(5):055705. 10.1088/2053-1591/aac255
54. Wei M, Sun L, Zhang C, Qi P, Zhu J (Jan. 2019) Shear-thickening performance of suspensions of mixed ceria and silica nanoparticles. J Mater Sci 54(1):346–355. 10.1007/s10853-018-2873-4
55. Galindo-Rosales FJ, Rubio-Hernández FJ, Sevilla A, Ewoldt RH (2011) How Dr. Malcom M. Cross may have tackled the development of 'An apparent viscosity function for shear thickening fluids,' *J Nonnewton Fluid Mech*, vol. 166, no. 23–24, pp. 1421–1424, Dec. 10.1016/j.jnnfm.2011.08.008

Figures

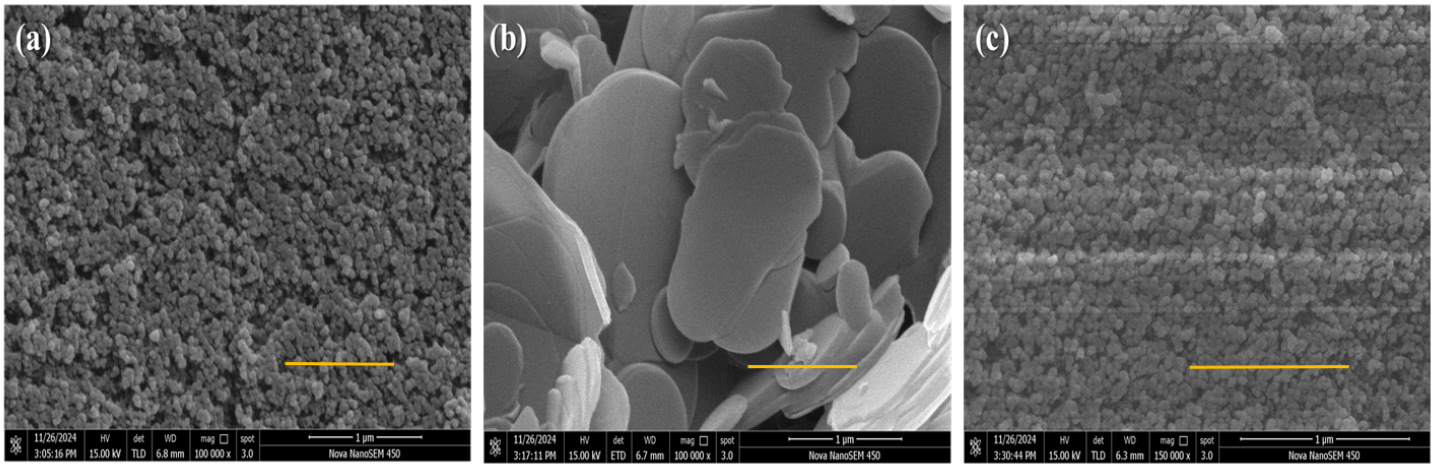

Figure 1

SEM micrographs showing the surface morphology of **(a)** nano-SiO_2 particles, (b) nano-h-BN particles, and (c) the nano-h-BN/SiO_2 composite.

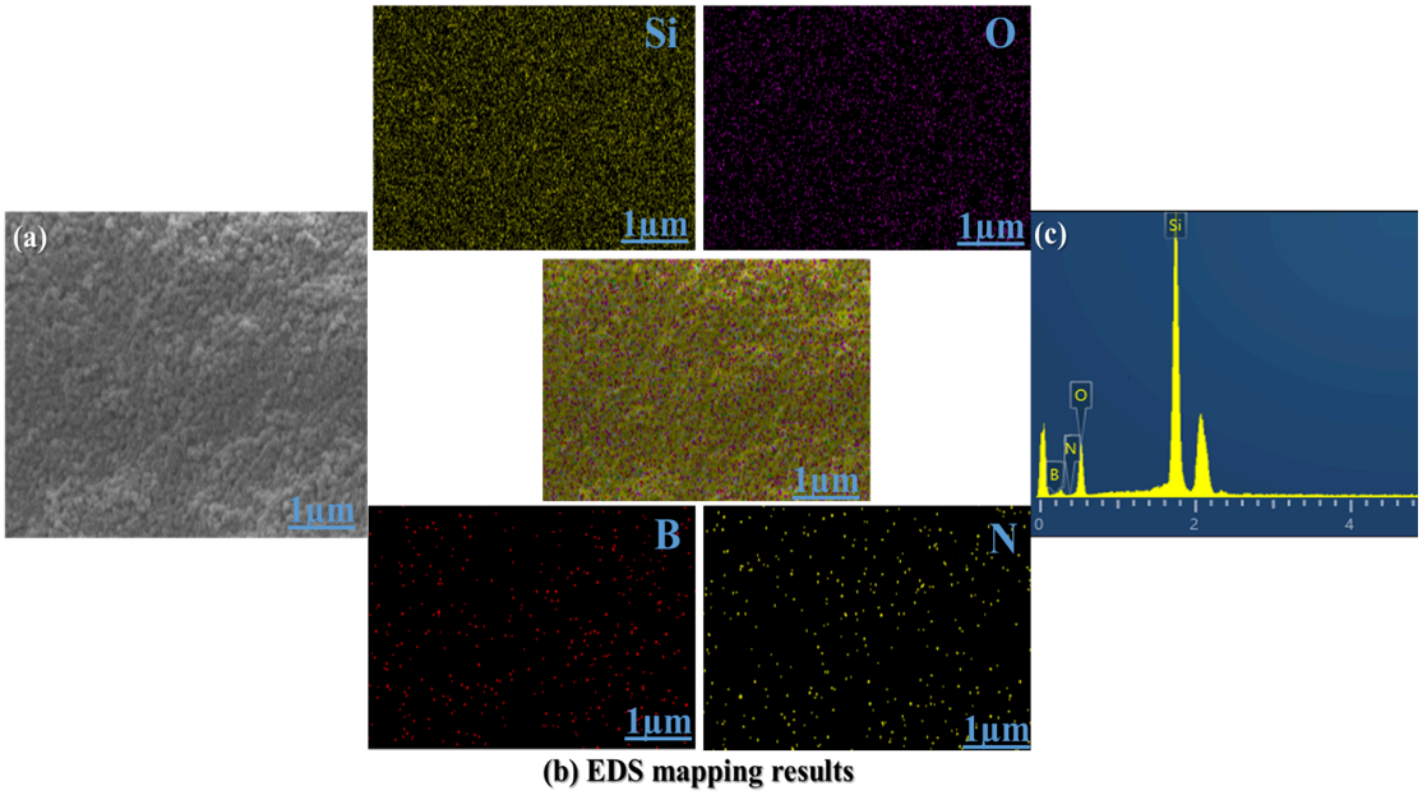

Figure 2

EDS characterization of the nano h-BN/SiO_2 composite sample with a mass fraction of 0.1%/15%: (a) selected EDS scan area, (b) corresponding elemental mapping results, and (c) EDS spectrum.

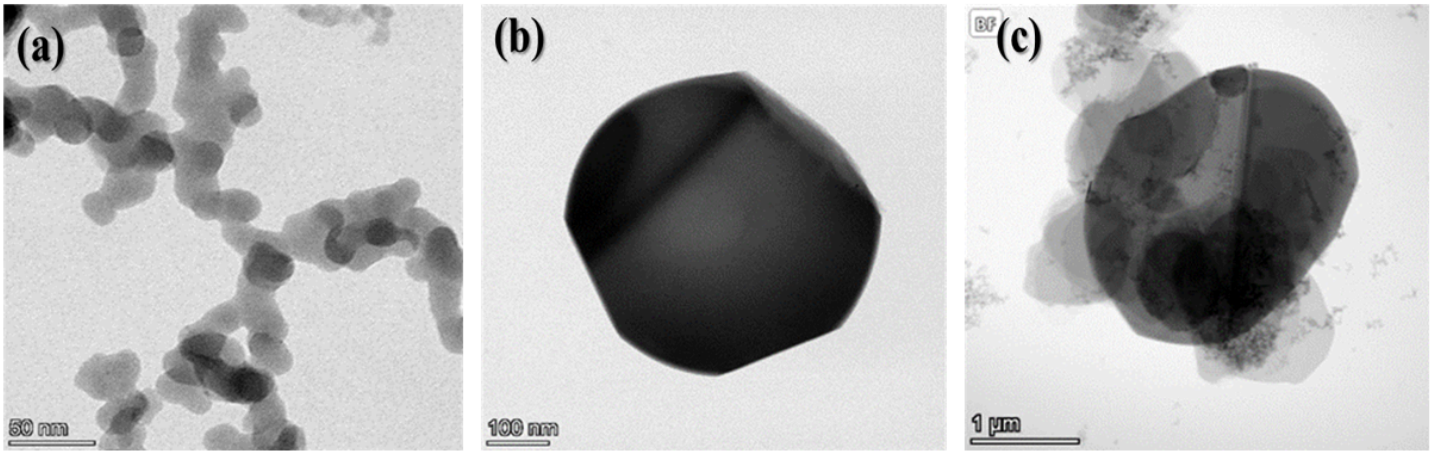

Figure 3

HR-TEM images of (a) SiO2 nanoparticles, (b) h-BN nanoparticles, and (c) nano h-BN/SiO_2 composite.

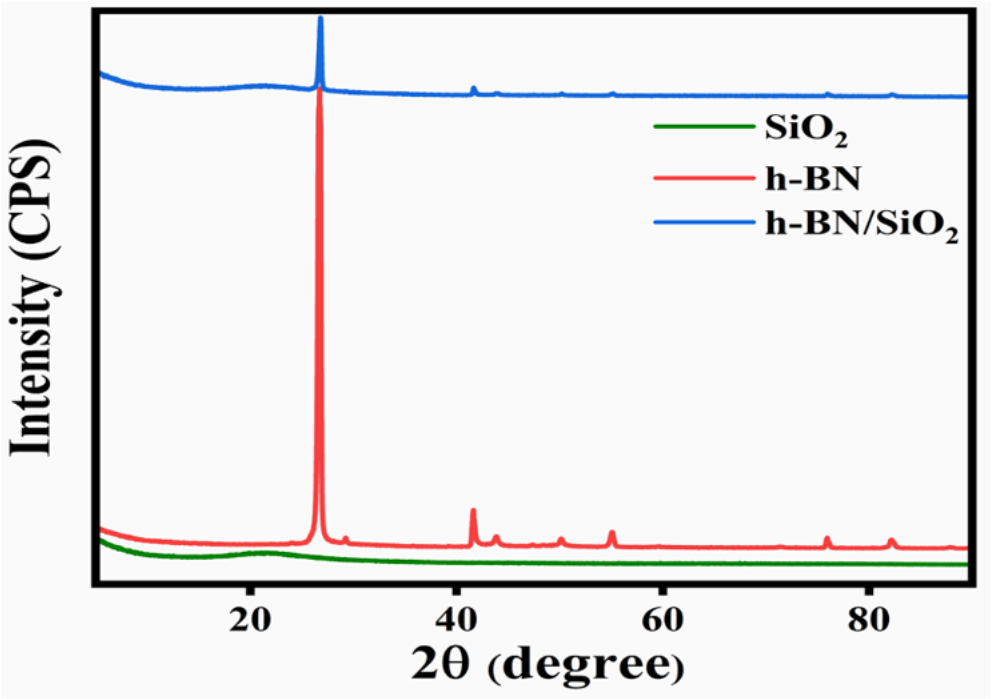

Figure 4

The XRD diffraction profile of SiO_2, h-BN, and h-BN/SiO_2 composite powders.

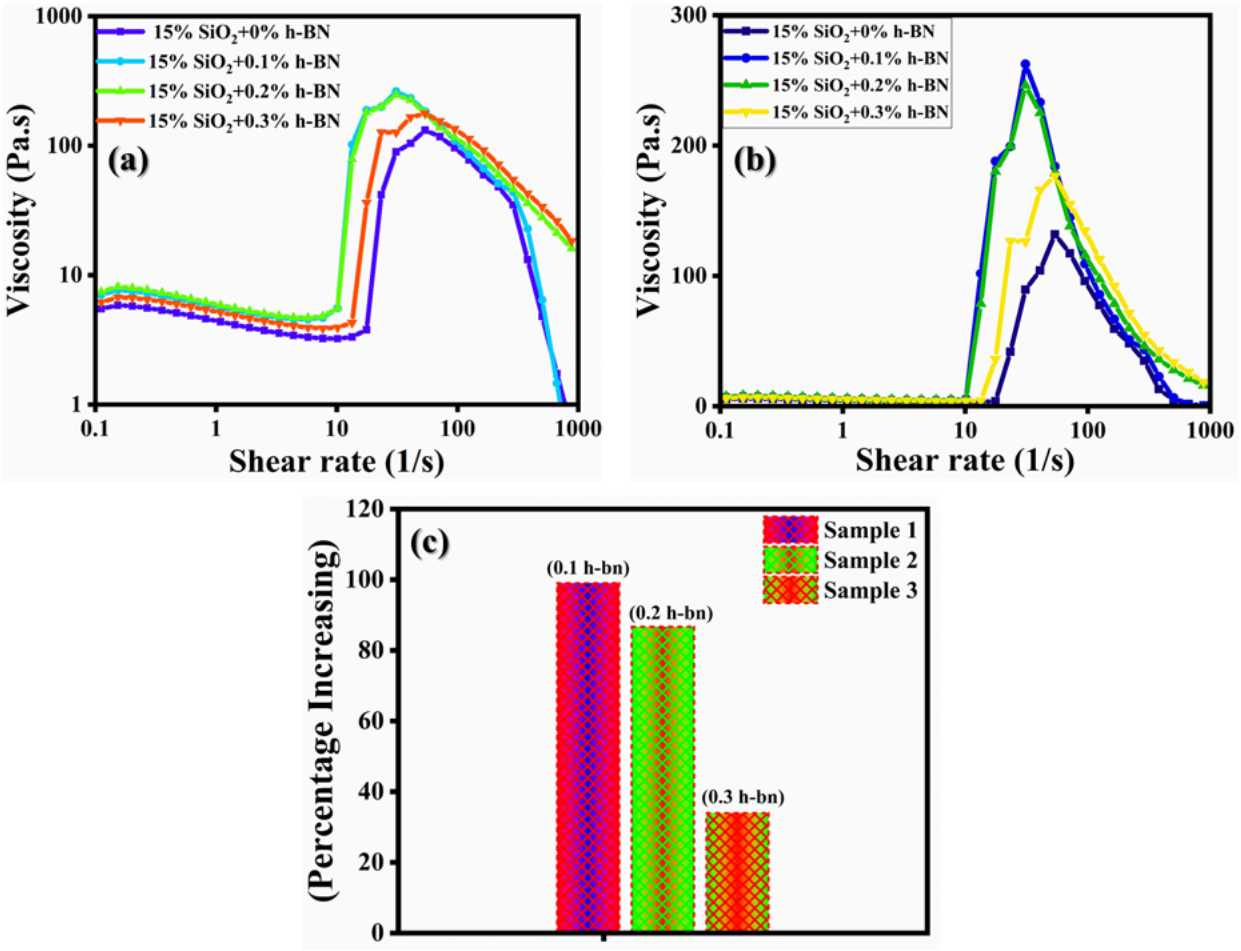

Figure 5

For the h-BN-SiO_2/STF system prepared with varying h-BN-to-SiO_2 ratios, viscosity vs shear rate is illustrated using (a) Log graph, (b) half Log graph, and (c) Comparative analysis for numerous h-BN shear-thickening fluids.

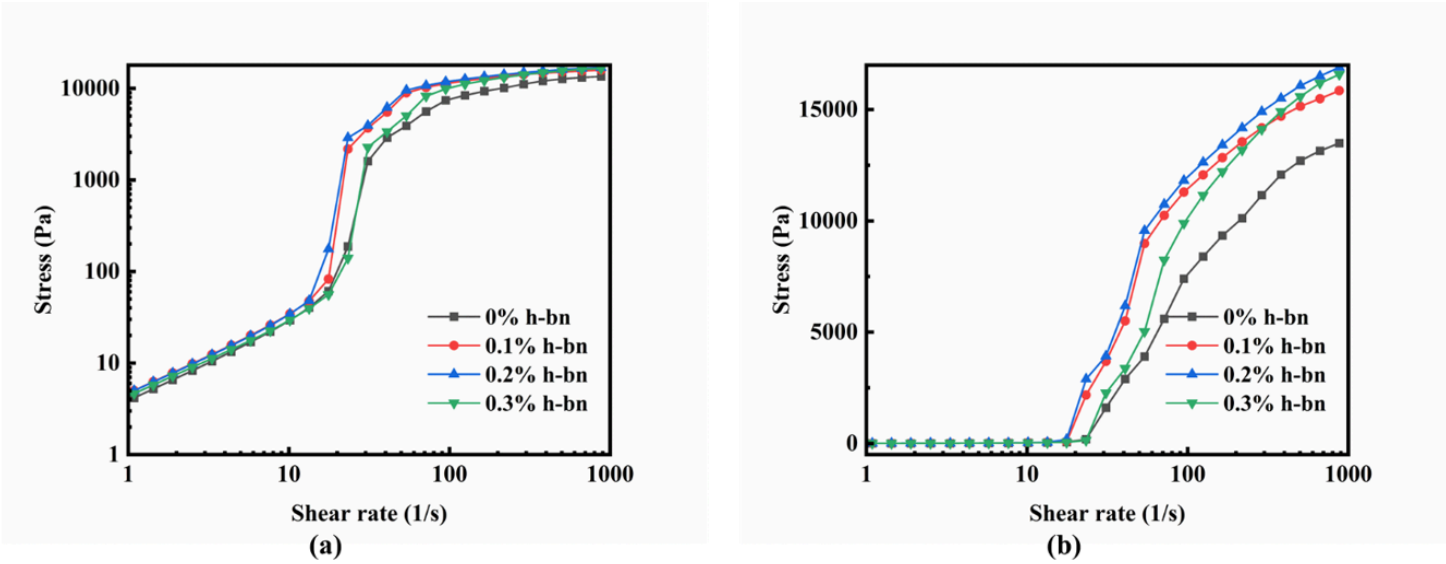

Figure 6

For the h-BN-SiO_2/STF system with different h-BN ratios, Stress against shear rate. (a) Logarithmic graph. (b) Semi-Logarithmic graph.

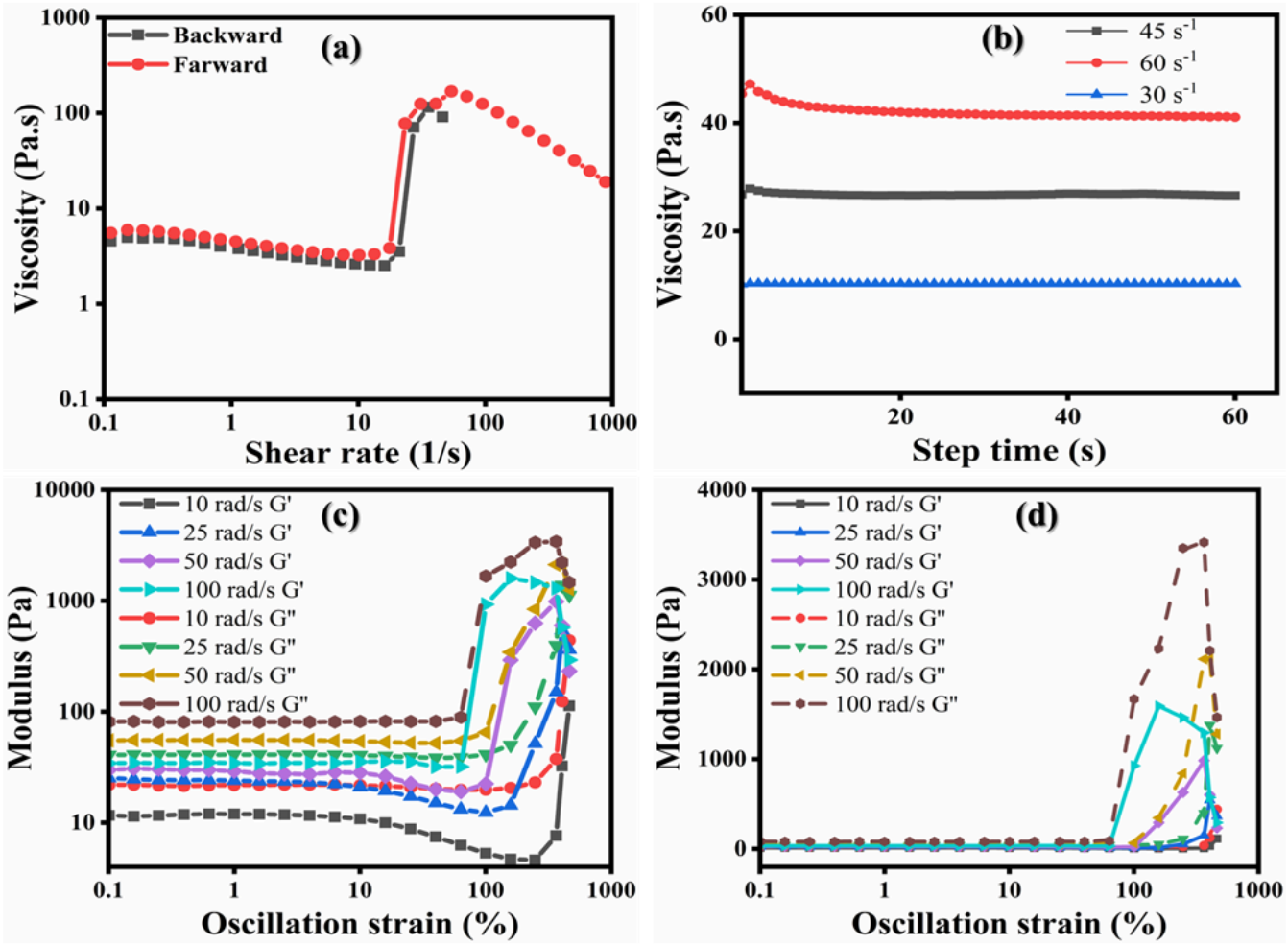

Figure 7

Rheological characteristics of the 0.1%h-BN/SiO_2-STF shear thickening fluid sample (a) Reversibility, (b) Stability, (c) Strain versus storage and loss modulus for 0.1%h-BN/SiO_2-STF Coordinate logarithm, and (d) Semi-coordinate Logarithm.

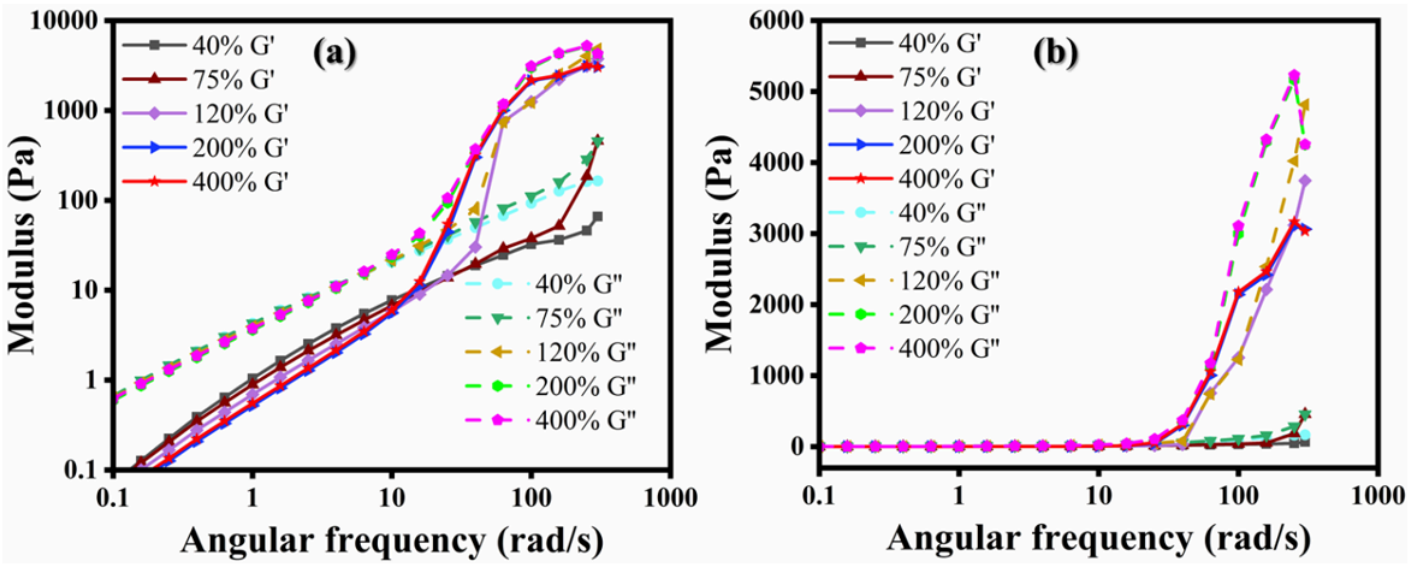

Figure 8

Storage and loss modulus for 0.1% h-BN/SiO_2-STF as a frequency function, (a) Logarithmic, and (b) Semi-logarithmic.

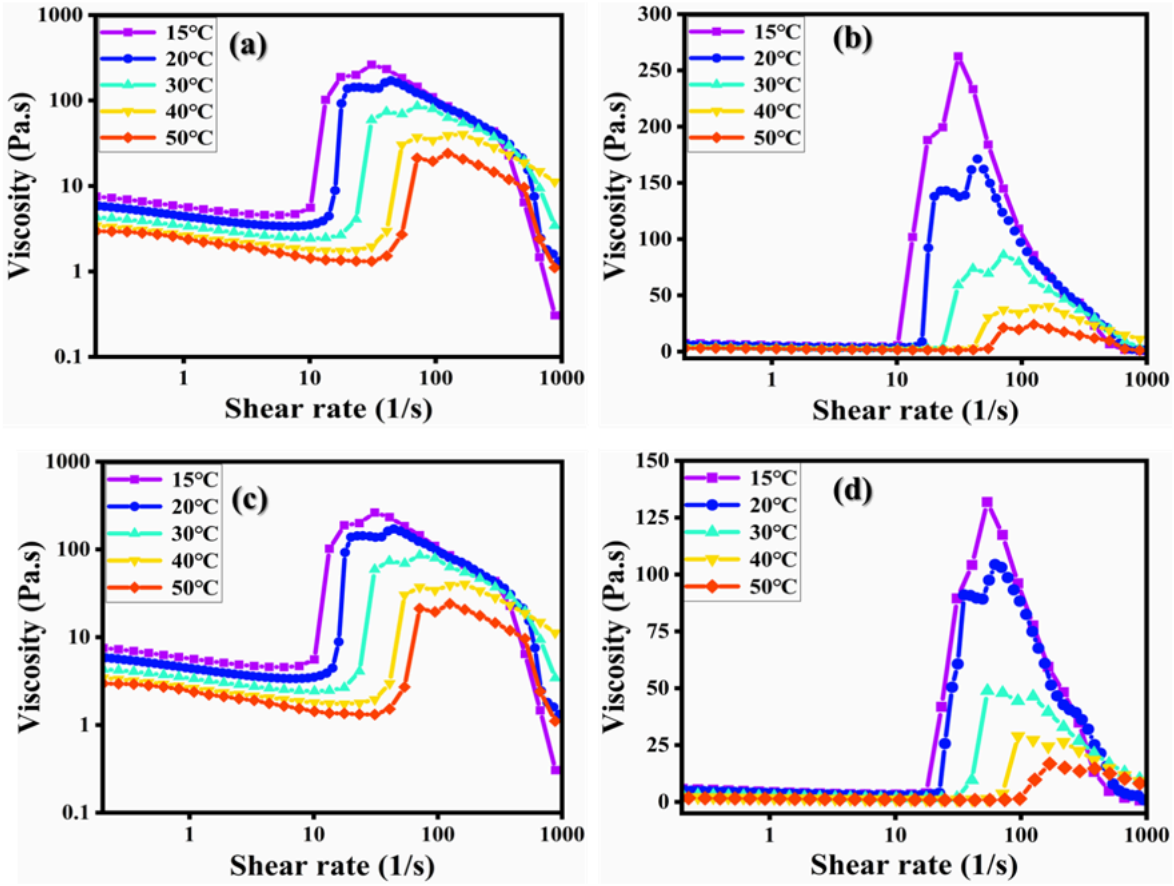

Figure 9

Shear rate against viscosity for 0.1%h-BN/SiO_2-STF. at different temperatures, (a) Logarithmic, (b) Semi-logarithmic, (c) Shear rate against viscosity for 0% h-BN/SiO_2-STF. to varying temperatures of coordinate. Logarithm, and (d) Semi-logarithmic.

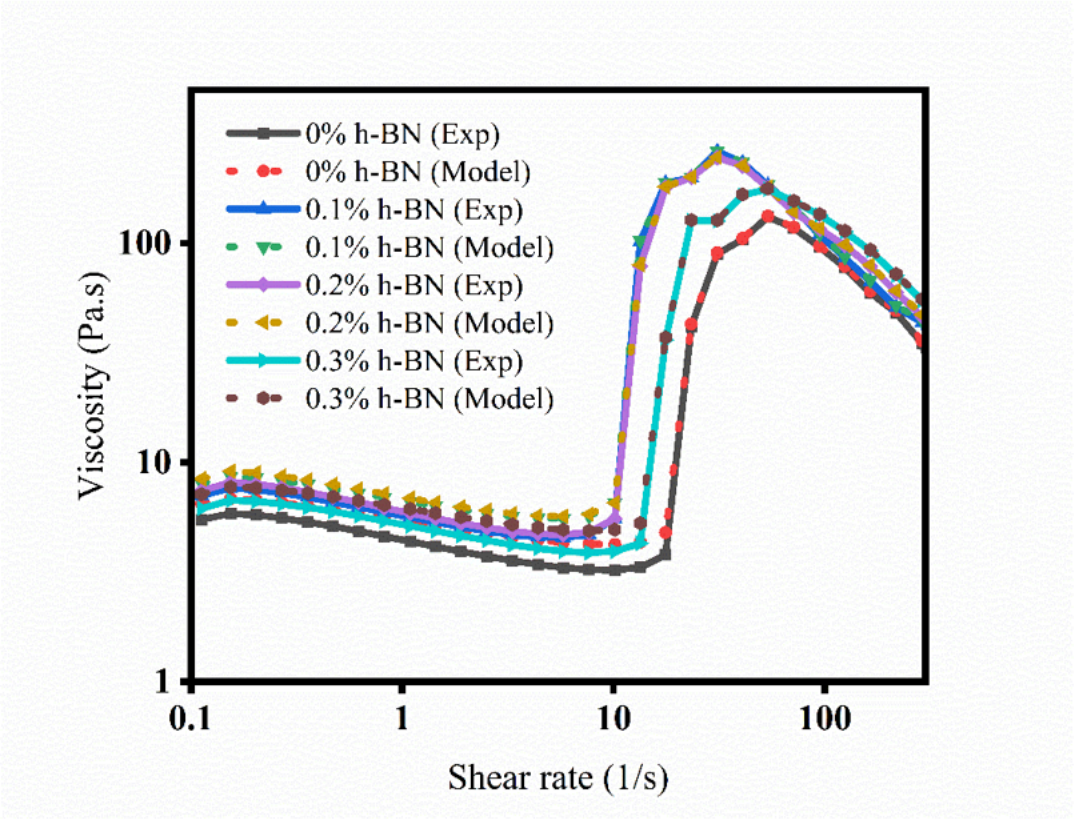

Figure 10

Comparison between experimental results and the model for various h-Bn percentages, including 0%, 0.1%, 0.2%, and 0.3%.